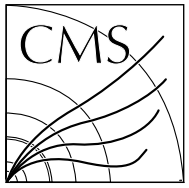

The Compact Muon Solenoid Experiment

CMS Note

Mailing address: CMS CERN, CH-1211 GENEVA 23, Switzerland

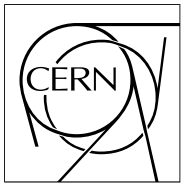

26 May 2006

Search with the CMS detector for heavy resonances decaying into an electron pair

B. Clerbaux, T. Mahmoud

ULB,Université Libre de Bruxelles, Brussels, Belgium

C. Collard, P. Miné

LLR,Ecole Polytechnique, Palaiseau, France

Abstract

This note presents the CMS experiment potential to discover heavy resonances decaying into an electron-positron pair, such as Kaluza-Klein excitations of Z or graviton bosons predicted in extra dimension models (the TeV^{-1} model and the Randall-Sundrum model), or neutral heavy Z' bosons predicted by Grand Unified Theories. Full and fast simulations of the CMS detector response and reconstruction program are used to investigate these productions, with pile-up conditions corresponding to a luminosity of $2 \times 10^{33}\ \mathrm{cm}^{-2}\mathrm{s}^{-1}$. For an integrated luminosity of 30 fb^{-1}, a 5σ discovery limit is obtained for a mass of 5.5 $\mathrm{TeV/c}^2$ in the case of Kaluza-Klein excitations of Z boson production. For Randall-Sundrum graviton production, the limits are masses of 1.6 $\mathrm{TeV/c}^2$ for a coupling parameter constant $c = 0.01$ and 3.8 $\mathrm{TeV/c}^2$ for $c = 0.1$. For the six Z' models considered here, the 5 σ discovery limits range from masses of 3.3 $\mathrm{TeV/c}^2$ (Z_ψ) to 4.3 $\mathrm{TeV/c}^2$ ($\mathrm{Z}_{\mathrm{ALRM}}$).

1 Introduction

Heavy resonances with masses above 1 $\mathrm{TeV/c^2}$ are predicted by several models beyond the Standard Model (SM), in particular models with extra spatial dimensions and Grand Unified Theories (GUT).

The existence of several "large" spatial extra-dimensions in which gravity propagates has been proposed by Arkani-Hamed, Dimopoulos and Dvali (ADD) [1] as a possible solution to the hierarchy problem. In their model, the observed three-dimensional space is a 3D-brane embedded in a higher dimensional space, the extra spatial dimensions (the bulk) being orthogonal to the 3D-brane. In this picture, the SM fields are localized on the 3D-brane, while the gravitational field spreads throughout the whole space. The Planck scale appears as an apparent scale, while the fundamental gravity scale is at the TeV level. In order not to introduce unobserved deviations from Newton's law, the extra dimensions should be of finite size. This is realized by a compactification mechanism, which leads to Kaluza-Klein (KK) excitations from fields propagating in the bulk. Several models have been proposed to explain the apparent hierarchy. A review is given in Ref. [2]. The ADD model has been extensively studied at LEP, HERA and Tevatron and prospective studies are carried at LHC (see the reviews presented at EPS2003 [3]).

1.1 The TeV^{-1} model

Models with extra dimensions of different sizes have also been proposed [4–6]. The gravitons are not the only particles possibly sensitive to extra dimensions. For example, gauge bosons could propagate in TeV^{-1}-sized extra dimensions. This possibility allows for new model building, which address gauge coupling unification [7] or fermion mass hierarchy [8]. The phenomenological consequence of this scenario is the appearance of a KK tower of states for gauge boson fields. The masses of the gauge boson modes are given by

$$M_n^2 = M_0^2 + n^2 M_{\mathrm{c}}^2 \tag{1}$$

where M_0 is the mass of the zeroth mode, corresponding to the SM fields, n is the mode number and M_{c} is the compactification scale, $M_{\mathrm{c}} = 1/R_{\mathrm{c}}$ (R_{c} being the compactification radius). In this approach, the existence of only one extra dimension, of radius $R_{\mathrm{c}} \simeq \mathrm{TeV}^{-1} \simeq 10^{-17}\mathrm{cm}$, compactified on a circle with an orbifold condition, (compactification on S^1/Z^2), is assumed. Two specific models are considered, leading to different interference terms between the SM gauge bosons and the KK excitations of the gauge bosons [5, 8]. In the first case (model M^+), all the SM fermions are localized at the same orbifold point. The couplings of fermions to KK gauge bosons are the same as in the SM, but scaled by a factor $\sqrt{2}$. In the second case (model M^-), quarks and leptons are localized at opposite fixed points. This implies that, compared to model M^+, the signs of the quark couplings to the bosons are reversed for excitations with n odd. The model M^+ (M^-) is characterized by a fully constructive (destructive) interference between the SM gauge bosons and KK excitations. These models have only one free parameter, the compactification scale M_{c}. The value of M_{c} is constrained by precise electroweak measurements, in particular the measurement of two fermions processes at LEP2. A conservative lower limit of 4 TeV for the compactification has been derived [6, 9].

1.2 The Randall and Sundrum model

Heavy resonances at high mass are also predicted in the framework of the Randall and Sundrum (RS) model [10] with only one extra dimension (Φ). The RS geometry is non-factorizable and based on a slice of a Anti-de Sitter (AdS_5) space-time. The extra dimension is compactified on a S^1/Z^2 orbifold, with fixed points $\Phi = 0, \pi$ holding two 3-branes. The gravity is localized on the brane at $\Phi = 0$, the gravity scale is given by

$$\Lambda_\pi = M_{\mathrm{Pl}}\, e^{-kR_c\pi} \tag{2}$$

where k is the AdS_5 curvature ($\sim M_{\mathrm{Pl}}$), R_c is the compactification radius and the exponential term is called the warp factor. The scale Λ_π can be of the order 1 TeV if $kR_c \simeq 11$ to 12 (with radion stabilization [11]). Therefore for $k \sim 10^{18}$ GeV, R_c should be $\sim 10^{-33}$ m. In the 4-dimension world, massive KK excitations of gravitons appear, with masses given by

$$M_n = kx_n e^{-kR_c\pi} \tag{3}$$

where x_n is the n^{th} root of the Bessel function J_1. The coupling of excited gravitons to matter is described by

$$L = -\frac{1}{\Lambda_\pi} T^{\mu\nu} \sum_{n=1}^{\infty} h_{\mu\nu}^{(n)} \tag{4}$$

where $T^{\mu\nu}$ is the energy-momentum tensor of the matter field, $h^{(n)}_{\mu\nu}$ is the n^{th} graviton excitation.

In the RS model, gravitons are massive resonances, with masses of order of $\mathrm{TeV/c^2}$. Their couplings to SM fermions and bosons are expected to be universal, and the decay branching fractions for masses $\sim$ 1 $\mathrm{TeV/c^2}$ depend essentially on the multiplicity of possible quantum states (spin, colour, flavour).

Two parameters control the properties of the RS model: the mass of the first KK graviton excitation, and the coupling constant $c = k/M_{\mathrm{Pl}}$ determining graviton couplings (see eq. 4) and widths:

$$\Gamma_n = \rho M_n x_n^2 c^2 \tag{5}$$

where ρ is a constant depending on the number of open decay channels.

Two theoretical constraints exist on these two parameters. The first is a limit on the curvature originally formulated in [10] as $k < M$, where $M \sim M_{\mathrm{Pl}}$ is the fundamental five-dimensional Planck scale. The second constraint, $\Lambda_\pi < 10$ TeV, assures that no new hierarchy appears between M_{EW} and Λ_π. The first direct constraints on RS graviton production come from the Tevatron Run II, excluding a graviton mass up to 535 $\mathrm{GeV/c^2}$ for $c = 0.1$ [12].

1.3 Z' gauge bosons

A number of possible extensions to the Standard Model, such as superstring-inspired $\mathrm{E_6}$ models [13] or left-right symmetry-breaking models [14], predict the existence of an extra heavy neutral gauge boson, generically called Z'. There are no reliable theoretical predictions, however, of the Z' mass scale. Currents lower limits on the Z' mass are (depending on the model) of the order of 600-900 $\mathrm{GeV/c^2}$ [15].

From a large variety of Z' bosons described in the literature, we chose six cases which are frequently discussed and whose properties are thought to be representative of a broad class of extra gauge bosons. They are the same as those studied for the Z' $\rightarrow \mu^+\mu^-$ channel [16]:

- $\mathrm{Z_{SSM}}$ within the Sequential Standard Model (SSM), which has the same couplings as the standard Model $\mathrm{Z^0}$ and is often used as a benchmark by experimentalists.
- $\mathrm{Z_\psi}$, $\mathrm{Z_\eta}$, and $\mathrm{Z_\chi}$, arising in $\mathrm{E_6}$ and SO(10) GUT groups.
- $\mathrm{Z_{LRM}}$ and $\mathrm{Z_{ALRM}}$, arising in the framework of the so-called "left-right" and "alternative left-right" models. Their couplings were calculated according to the formalism in Ref. [14] with $g_R = g_L$.

1.4 Heavy resonance production at LHC

The LHC will provide sufficiently high energy in the centre of mass to allow the CMS experiment to search for the direct production of new heavy resonances predicted by the three models presented above, when kinematically accessible. Note that, for a heavy Z signal, if $M_{\mathrm{n}} \gg \hat{s}$, KK excitation of gauge bosons may still be discovered through the observation of deviations in the Drell-Yan distribution coming from the interference between the SM and the KK excitations of gauge bosons. In this note, we nevertheless focus on the direct search for the first KK excitation M_1, called M in the rest of the paper. In the case of KK excitation of Z bosons, only the $\mathrm{M^+}$ model is considered, as the difference between the $\mathrm{M^+}$ and the $\mathrm{M^-}$ models is expected only in the interference region, at masses lower than the first resonance. The main discovery channel comes from the observation of the decay of a heavy particle into an electron pair, which presents a clear resonance signature over a well controlled Drell-Yan background.

Once a heavy resonance is discovered, its observables can be used to characterise the theoretical framework to which its belongs. The measurements of angular distributions and forward-backward asymmetries of the leptonic decay products, both at the resonance peak and off the peak, provide powerful tools to disentangle gravitons (spin 2) from KK Z or Z' bosons, and even to identify the Z'. Angular distribution studies require higher integrated luminosity than available in the first phase of data taking at the LHC. Nevertheless, a study of the possibility of disentangling different models is presented in Section 6, with integrated luminosities of 100 and 300 $\mathrm{fb^{-1}}$.

In CMS, several studies were already performed on the search for heavy resonances. For heavy graviton search in the RS model framework, an analysis using the full CMS detector simulation was performed in [17]. A recent analysis on the search for graviton decaying into a photon pair in given in Ref. [18]. The CMS discovery potential of a heavy Z boson from Grand Unified Theory was studied in detail in the di-muon decay channel in [16]. Angular studies have been performed in Refs. [17] and [19].

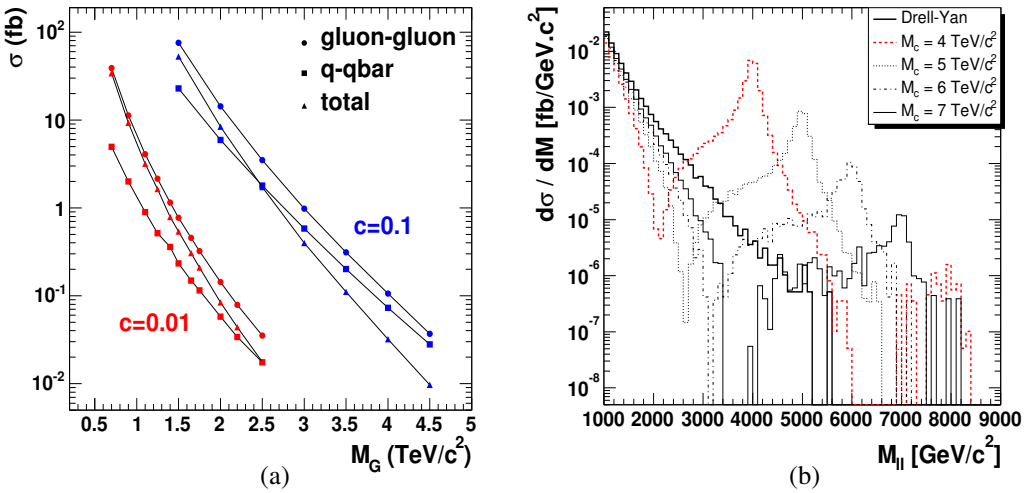

Figure 1: (a) Cross section for $\mathrm{pp} \to \mathrm{G} \to \mathrm{e^+e^-}$ production (circles), for different values of c ($c = 0.01$ in red and $c = 0.1$ in blue) in units of 10^{-13} mb. The contributions from $\mathrm{q\bar{q}}$ and gluon-fusion are displayed with squares and triangles, respectively. (b) Differential KK gauge boson production cross section as a function of the di-lepton mass, for four compactification scales: the dashed, dotted, dash-dotted and thin full line distributions correspond to $M = 4, 5, 6$ and 7 $\mathrm{TeV/c^2}$, respectively, for the M^+ model, using a number of modes $n = 4$. The thick full line shows the Drell-Yan background.

This note is organized as follows. The signal and background generations are presented in Section 2. The simulation of the CMS detector is given in Section 3, which includes a presentation of tools needed in the context of high energy electrons in the final state: energy and electromagnetic calorimeter electronic saturation corrections. The selection criteria are given in Section 4. The mass reconstruction and the CMS experiment discovery potential are discussed in Section 5. Studies of the electron angular distribution in view of identifying the new particle are given in Section 6. Finally, a discussion on the systematic effects is given in Section 7.

2 Signal and background generation

At parton level, heavy Z bosons can be resonantly produced at the LHC via the channel $\mathrm{q\bar{q}} \to \mathrm{Z}$, and heavy gravitons via $\mathrm{q\bar{q}} \to \mathrm{G}$ and $\mathrm{gg} \to \mathrm{G}$. The generation of proton-proton collisions at 14 TeV centre of mass energy is done with the program CMKIN.4.1.0 interfaced to PYTHIA 6.227 [20] with the choice of the CTEQ 6.1M proton parton distribution set [21].

The process numbers ISUB=391 and 392 are chosen in PYTHIA for graviton production and ISUB=141 for Z' production. The event generation with PYTHIA includes the full $\gamma^*/\mathrm{Z}^0/\mathrm{Z}'$ interference structure. The usual assumption is made that Z' bosons decay only to the three ordinary families of quarks and leptons and that no exotic decay channels are open. The KK gauge boson production is computed at the parton level with matrix elements, interfaced to PYTHIA as an external process, including the full interference structure and angular informations for decay products [5].

For the three models, the program PHOTOS 2.3 [22] is used for inner Bremsstrahlung production. The initial parameter value is taken as 0.01 for the limit of photon energy fraction, with the implementation of double Bremsstrahlung.

The SM background for the three models consists mostly of the Drell-Yan process, $\mathrm{q\bar{q}} \to \gamma/\mathrm{Z} \to \mathrm{e^+e^-}$. This background can be simulated in two ways, either using the KK code with only SM γ and Z boson exchange ($n = 0$) or using the PYTHIA generator with the standard option for Drell-Yan production (ISUB=1). It was checked that the KK and the PYTHIA generators give the same absolute cross section and the same distributions of the main kinematic variables. A factor 4/3 was missing in the KK gauge boson cross section calculation in Ref. [6] and is corrected for in the present analysis.

The cross section for graviton production, $\mathrm{pp} \to \mathrm{G} \to \mathrm{e^+e^-}$, is given in Fig. 1(a) for two values of c, in units of 10^{-13} mb. The contributions from $\mathrm{q\bar{q}}$ and gluon-fusion are displayed with squares and triangles, respectively. The

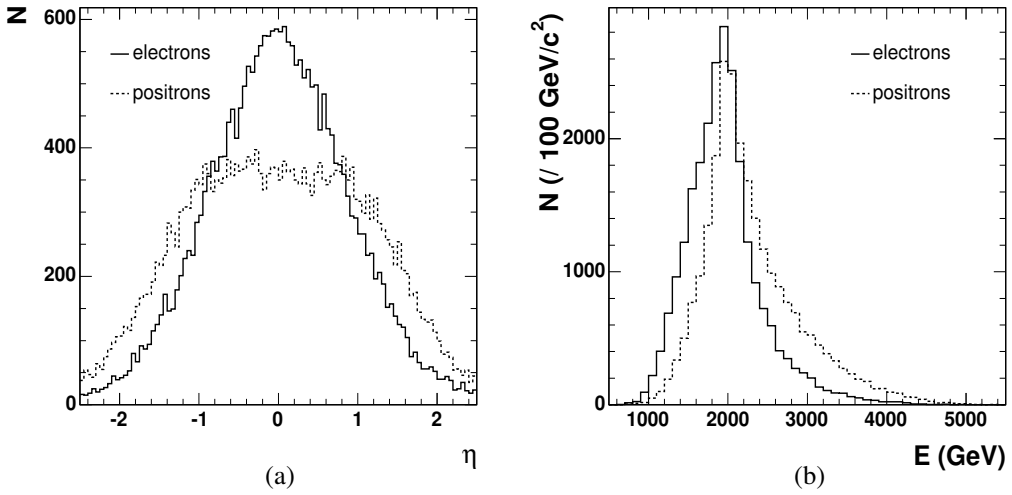

Figure 2: Distributions for signal events, $q\bar{q} \rightarrow (\gamma^{(n)} / Z^{(n)}) \rightarrow e^+e^-$, generated with $M = 4$ TeV/c^2 and $n = 4$: (a) pseudo-rapidity and energy (b) for decay positrons (dotted line) and electrons (full line).

differential cross section for KK Z boson production is given in Fig. 1(b) as a function of the di-lepton invariant mass, for the Drell-Yan background and for four different compactification masses ($M = 4$, 5, 6 and 7 TeV/c^2) for the M^+ model with the number of modes $n = 4$. The distributions show the peaks centered at M, corresponding to the superposition of the $\gamma^{(1)}$ and $Z^{(1)}$ Breit-Wigner shapes. The low mass region corresponds to the SM γ and Z boson exchange and their negative interference with the KK gauge bosons in the M^+ model. Only the first four resonances are taken into account in the KK Z production cross section. Although this procedure does not alter the results in the peak region, it significantly modifies the number of expected events at low mass in the interference region.

The cross sections decrease with the increase of the heavy Z boson or graviton mass, and in the graviton case, with the decrease of the c parameter.

The cross sections and the numbers of generated events for the three models under consideration are given in Table 1. In the case of heavy Z production, the events are generated above some lower threshold of the di-lepton invariant mass (M_t), of which the values are also given in the table. The events are generated in the region $|\eta| < 2.5$. The cross sections obtained for Z' production and for the Drell-Yan process are similar to those in [16].

For KK Z boson production, an example of the main kinematic distributions (at the generated level) in the hadronic pp centre of mass frame is shown in Fig. 2. The η and energy distributions of the positive lepton are different from those of the negative lepton. This charge asymmetry is characteristic of the V-A coupling of the Z boson in the $q\bar{q}$ frame, convoluted with a boost, in the $+z$ or $-z$ direction, from the partonic centre of mass system to the hadronic frame. The η distributions are symmetric around zero, showing no preferred direction in the pp collision.

For KK Z and Z' boson production, a K factor of 1.0 is used for both the signal and the Drell-Yan background, since heavy Z production interferes with Z/γ Drell-Yan production. For the graviton analysis, as little interference is expected with the SM processes, a K factor of 1.0 is used for the signal and of 1.3 for the Drell-Yan background, in order to take into account the higher order terms in the cross section. The latter number comes from the CDF analysis [12] and is compatible with the K factor obtained from theoretical computations [23].

3 Simulation of the CMS detector

The generated events were passed through a detailed simulation of the CMS detector (OSCAR code, version 3.6.5 and ORCA code, version 8.7.3). The detector full simulation was performed for KK Z boson production at $M = 4$ and 6 TeV/c^2, and for graviton and Z' production at $M = 1.5$ and 3.5 TeV/c^2, with at least 5000 events per parameter set. Additional samples at various masses were produced using the fast simulation (FAMOS code, version 1.3.2), as detailed in Table 1. Both for ORCA and FAMOS simulations, pile-up events were added, according to the low luminosity phase conditions ($L = 2 \times 10^{33}$ cm^{-2}s^{-1}).

Table 1: Processes generated with PYTHIA: cross sections (in fb) and number of generated events. The masses M and the mass thresholds M_{t} are given in $\mathrm{TeV/c^2}$.

Mass	Model parameter	Cross-section (fb)						N (10^3)	simulation
KK Z boson production: $\mathrm{pp} \to \mathrm{KKZ}/\gamma \to \mathrm{ee}$									
$M = 4.0$	M_{t}=2.5	2.46						20	ORCA
$M = 6.0$	M_{t}=4.0	0.0539						5	ORCA
$M = 4.0$	M_{t}=2.5	2.46						50	FAMOS
$M = 4.5$	M_{t}=3.0	0.937						50	FAMOS
$M = 5.0$	M_{t}=3.5	0.359						50	FAMOS
$M = 5.5$	M_{t}=3.5	0.142						50	FAMOS
$M = 6.0$	M_{t}=4.0	0.0539						50	FAMOS
Graviton production: $\mathrm{pp} \to \mathrm{G} \to \mathrm{ee}$									
$M = 1.50$	c =0.01	0.930						10	ORCA
$M = 3.50$	c =0.1	0.367						10	ORCA
$M = 0.75$	c =0.01	31.0						5	FAMOS
$M = 1.00$	c =0.01	7.85						5	FAMOS
$M = 1.25$	c =0.01	2.45						5	FAMOS
$M = 1.50$	c =0.01	0.930						5	FAMOS
$M = 1.75$	c =0.01	0.389						5	FAMOS
$M = 2.00$	c =0.01	0.175						5	FAMOS
$M = 2.00$	c =0.1	17.3						5	FAMOS
$M = 2.50$	c =0.01	0.042						5	FAMOS
$M = 2.50$	c =0.1	4.19						5	FAMOS
$M = 3.00$	c =0.1	1.18						5	FAMOS
$M = 3.50$	c =0.1	0.367						5	FAMOS
$M = 4.00$	c =0.1	0.125						5	FAMOS
$M = 4.50$	c =0.1	0.043						5	FAMOS
Z' production: $\mathrm{pp} \to \mathrm{Z}' \to \mathrm{ee}$		SSM	ψ	η	χ	LRM	ALRM		
$M = 1.5$	M_{t}=1.0	86						10	ORCA
$M = 3.5$	M_{t}=2.75	0.62						10	ORCA
$M = 1.0$	M_{t}=0.4	521	275	293	414	422	614	5	FAMOS
$M = 3.0$	M_{t}=1.5	2.29	1.38	1.47	1.8 9	1.95	3.09	5	FAMOS
$M = 5.0$	M_{t}=3.0	0.038	0.025	0.027	0.030	0.032	0.060	5	FAMOS
Drell-Yan production: $\mathrm{pp} \to \gamma/\mathrm{Z} \to \mathrm{ee}$									
	M_{t}=2.5	0.0651						10	ORCA
	M_{t}=3.5	0.00630						10	ORCA
	$0.4 - 1.6$	173						5	FAMOS
	$0.65 - 1.0$	26.4						5	FAMOS
	$0.9 - 1.6$	8.51						5	FAMOS
	$1.3 - 3.0$	1.845						5	FAMOS
	$1.5 - 4.5$	0.947						5	FAMOS
	$2.7 - 5.0$	0.0333						5	FAMOS
	$3.0 - 7.0$	0.0163						5	FAMOS

3.1 Trigger

For the topology studied in this note the main trigger is based on the detection of large p_t electrons in the electromagnetic calorimeter ECAL. The trigger efficiency is expected to be very high due to the presence of two electrons with very large transverse energy in the final state. As the level 1 energy deposit in the ECAL trigger towers is coded on 7 bits of 0.5 GeV, the electron trigger will be energy saturated at 63.5 GeV. The trigger efficiency was checked for KK Z boson production at $M = 4$ TeV/c^2 and at $M = 6$ TeV/c^2. For $M = 4$ TeV/c^2, all events passed the L1 requirement of at least one isolated electromagnetic tower, and 98.7% that of double isolated electromagnetic towers. The efficiency at the high level trigger (HLT) level is 99.7% for single photon, 97.5% for double photon, and 93.3% for single electron. The efficiency is higher for photons than for electrons, because of additional conditions in the latter case, in particular track association to the electromagnetic cluster. Requiring a single isolated electromagnetic tower at L1 level and single photon at the HLT level, keeps 99.7% of the generated events. The trigger efficiencies are similar at $M = 6$ TeV/c^2. Note that these numbers are obtained without any selection cuts.

3.2 Energy reconstruction

The detection of two electromagnetic clusters is requested for this analysis. They are reconstructed as superclusters (SC) in the CMS electromagnetic calorimeter ECAL with the standard Hybrid algorithm [24] in the barrel region ($|\eta| < 1.442$) and Island algorithm in the endcap region ($1.566 < |\eta| < 2.5$). The algorithms were not specially optimised for very energetic electrons or photons. The energy deposits in the Pb-Si preshower calorimeters placed in front of the endcaps are included in the measurement. The two SC with the highest energy are selected as the electron candidates.

An important characteristic of the signal events is that the very energetic final state electrons may have a significant energy leakage beyond the ECAL. The energy deposit in the CMS hadronic calorimeter (HCAL) cell behind the ECAL cluster is included in the measurement, event by event. This procedure leads to an improvement of the energy determination, as shown by the study of single electron and photon calibration files at fixed energy.

The measured energy, including preshower and HCAL measurements, called $E_{\rm SC}$ in the following, is smaller than the generated energy. A dependence of the ratio $E_{\rm SC}/E_{\rm true}$ with η is also observed. The effect is visible in Fig. 3(a) for KK Z boson production at $M = 4$ TeV/c^2. At low energy (less than 100 GeV), it has been cured for the Hybrid SC algorithm in the barrel by performing a correction depending on the number of crystals. Applying the same coefficients at high energy leads to an overestimate of the reconstructed electron energy. Correction factors for electron energy have therefore been determined using calibration files. The correction is extracted in 10 bins in $|\eta|$ and for 10 different energies. As an example, for $E = 500$, 1000, 2500 and 4000 GeV, the correction factors at $\eta = 0$ (in the barrel) are 0.973, 0.972, 0.967 and 0.961, respectively. The corresponding factors at $\eta = 2$

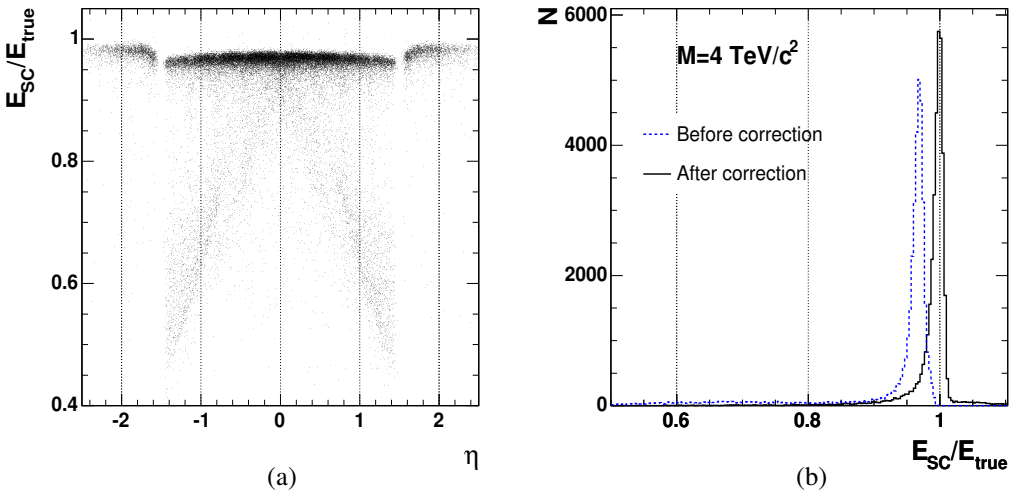

Figure 3: (a) Dependence in η of the ratio $E_{\rm SC}/E_{\rm true}$; (b) Ratio $E_{\rm SC}/E_{\rm true}$ before (dashed line) and after (full line) energy correction, for KK Z boson production with M =4 TeV/c^2. The few events with a low value of $E_{\rm SC}/E_{\rm true}$ correspond to events for which the read-out of the highest energy crystal saturates (see next section).

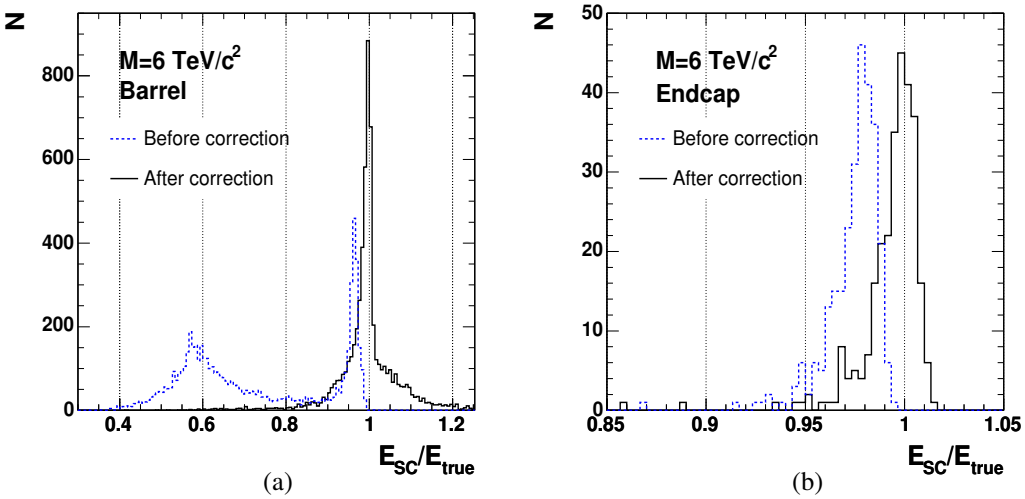

(a) (b)

Figure 4: Ratio E_{SC}/E_{true} for electrons in the barrel (a) and in the endcap (b), before (dashed line) and after (full line) energy correction, for KK Z boson production with $M = 6$ TeV/c^2.

(in the endcaps) are 0.983, 0.983, 0.983, 0.981.

After energy correction, as obtained from the calibration files, the resolution on the reconstructed SC energy is around 0.6% and the ratio $E_{\rm SC}/E_{\rm true}$ peaks at one as shown in Fig. 3(b) for KK Z boson production with $M = 4$ TeV/c^2. The small number of events with a $E_{\rm SC}/E_{\rm true}$ ratio between 0.5 and 0.9 corresponds to events for which the read-out of the highest energy crystal has saturated (see next section).

3.3 Saturation

For very energetic electrons and photons, saturation occurs in the ECAL single crystal electronics because of the limited dynamical range of the Multi-Gain-Pre-Amplifier [25]. From 2004 test beam data analysis, the saturation threshold has been established to be at 1.7 TeV in the barrel crystals and 3.0 TeV for the endcaps. The ECAL saturation is not presently included in the simulation (ORCA/FAMOS), and was implemented for this study in the barrel only. Crystals with electronics saturation in the barrel are discarded for energy measurement and methods to correct for this effect have been studied in [26] using electron and photon calibration files. The methods are based on the energy deposit in crystals surrounding the saturated crystal. The correction leads to the correct estimate of energy deposit with a resolution of around 7%. In addition, dedicated corrections, depending both on the electron energy and η, are performed for remaining losses.

The ratio $E_{\rm SC}/E_{\rm true}$ for KK Z boson production at $M = 6$ TeV/c^2 is given in Fig. 4(a) for the electrons in the barrel and in Fig. 4(b) in the endcap. The dashed lines and the full lines represent, respectively, the distributions before and after saturation and energy correction. The peak at lower $E_{\rm SC}/E_{\rm true}$ ratio in the barrel (dashed distribution) correspond to events for which electronics saturation occurred.

4 Selection criteria

The selected events must fulfill the trigger criteria (see Section 3.1) up to level 2.5. At least 2 SC with transverse momenta greater than 100 GeV/c are required in the ECAL ($|\eta| < 1.442$ or $1.566 < |\eta| < 2.5$).

Different selection cuts are applied, in view of their rejection efficiency on background samples, of charged pions, neutral pions and multi-jet, as described in Ref. [17].

To eliminate background from isolated charged hadrons, a cut is applied on the ratio of the HCAL to ECAL energies, $H/E < 0.1$, using respectively the energy deposit in the HCAL cell located just beyond the ECAL SC seed and the energy of the ECAL SC seed. The distribution of the H/E ratio is given in Fig. 5(a) in the case of KK Z boson with $M = 4$ TeV/c^2.

Table 2: Efficiency of the selection criteria for three heavy resonance production models and for Drell-Yan production; the resonance masses M and the mass windows are given in $\mathrm{TeV/c^2}$.

	KK Z	G	SSM Z'	DY
	$M = 4$ [3.5 - 4.5]	$M = 2$ $c = 0.01$ [1.901 - 2.082]	$M = 5$ [4.2-5.8]	[3.5 - 4.5]
2 SC in ECAL	0.93	0.91	0.89	0.94
Isolation	0.91	0.92	0.95	0.93
HCAL/ECAL ratio	0.96	0.98	0.98	0.96
Track association	0.95	0.96	0.96	0.95
Final efficiency	0.78	0.80	0.79	0.80

In order to reduce the background from multi-jet events, the two SC must fulfill the following isolation condition: the total transverse energy in a cone of radius $0.1 < \Delta R < 0.5$, with $\Delta R = \sqrt{\Delta\eta^2 + \Delta\phi^2}$, called E_{cone}, must be below $0.02\ E_{SC}^T$, where E_{SC}^T is the SC transverse energy. The distribution of the isolation variable $I_{Et} = E_{\mathrm{cone}}/E_{SC}^T$ is given in Fig.5(b) in the case of KK Z boson production with $M = 4\ \mathrm{TeV/c^2}$.

To reject neutral particles, a track is requested to be associated for each electron candidate. For some events, a final state radiation (FSR) photon may give rise to the second most energetic cluster, which might lead to event loss. To overcome this problem the following condition is applied: if a track is associated with only one of the two highest energy SC, the event is kept if it contains a third SC with $E > 300$ GeV, satisfying the H/E and isolation cuts described above, and with an associated track. No track sign condition is requested at this stage.

The signal efficiency for the three heavy resonance production models is presented in Table 2, for events generated in a defined mass window. For graviton, characterized for small couplings by a narrow resonance width and for Z' production, the mass window is taken as $\langle M \rangle \pm 3\sigma$, where $\langle M \rangle$ and σ are the mean and the standard deviation of a Gaussian fit on the peak of the $\mathrm{e^+e^-}$ invariant mass distribution after reconstruction (see end of the section). For the KK Z boson production, a fixed mass window (slightly asymmetric) is used, as given in Table 2.

The following corrections are then applied to the selected events:

- HCAL and preshower energy deposits: the energy deposits in the HCAL and, for the endcaps, in the preshower are included in the energy determination, event by event.
- Saturation correction: for showers with energy deposit $E_1 > 1.7$ TeV in a single crystal of the barrel,

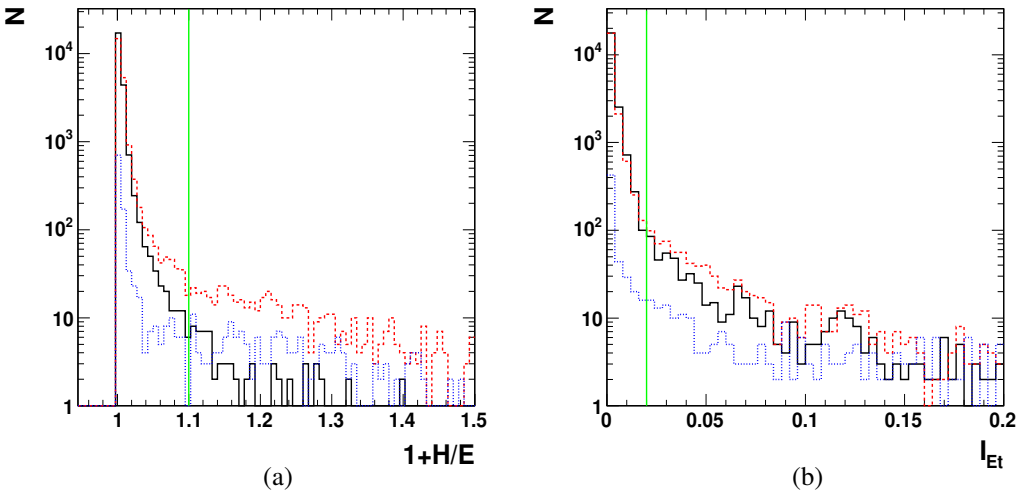

(a) (b)

Figure 5: Distribution of the $1 + H/E$ variable (a) and the isolation variable I_{Et} (b), for KK Z boson production with $M = 4\ \mathrm{TeV/c^2}$, for the highest energy SC (full line), the second SC (dotted line) and the third highest SC energy (dashed line).

electronics saturation is simulated and corrected for, see section 3.3.

- Energy correction: the measured energy is corrected using the method defined in section 3.2, depending on energy, η and whether electronics saturation occurs or not.
- z-vertex correction: to improve the vertex reconstruction resolution, the vertex interaction point is refitted using only the 2 electron tracks, instead of using all tracks as done by the default primary vertex reconstruction algorithm. The measurement in η is improved.
- Final State Radiation recovery: the event may contain a third energetic SC due to hard photon emission from Final State Radiation. If a SC with $E > 300$ GeV is present in the event, satisfying the H/E and isolation cuts described above, and close to one of the electron candidates ($\Delta R < 0.1$), this third SC is associated to the corresponding electron measurement.

An important point in the search for heavy new resonances is a precise measurement as precisely of the di-electron mass spectrum. Figures 6(a) and (b) show the mass distribution before and after energy correction, in the case of KK Z boson production at $M = 4$ and $M = 6$ TeV/c^2. The corresponding ratios $M_{\rm ee}/M_{\rm true}$ are given in Figs. 6(c) and (d). The peaks at low values of $M_{\rm ee}/M_{\rm true}$ correspond to events with crystal electronics saturation. The ratio $M_{\rm ee}/M_{\rm true}$ is slightly shifted toward lower masses (few per mill effect). This is due to the fact that the distribution of the electron energy ratio, $M_{\rm SC}/M_{\rm true}$, peaks at 1.0, but is slightly asymmetric around the peak. The final resolution obtained on the resonance mass is around 0.6% for events with no crystal electronics saturation and around 7% for events with saturation.

5 Results

5.1 Mass distributions

The invariant mass is reconstructed from the energy and angles of the 2 highest energy SC after the selection cuts and corrections mentioned above. The number of signal events N_S and the number of background events N_B are computed for the mass windows defined in Section 4. Figure 7 presents the signal over background for KK Z boson production with $M = 4$ and $M = 6$ TeV/c^2, for an integrated luminosity of 30 fb^{-1}; Figure 8 for Z' production with $M = 1.5$ and $M = 3.5$ TeV/c^2; Figure 9 for graviton production with $M = 1.5$ TeV/c^2, $c = 0.01$ and with $M = 3.5$ TeV/c^2, $c = 0.1$. For the three models, the peak is clearly visible over the background.

5.2 ORCA-FAMOS comparison and pile-up effects

The fast simulation FAMOS is used for some of the MC samples. Detailed comparison have shown no significant discrepancies between full simulation and fast simulation for the key variables used in this analysis and in terms of overall efficiencies.

The simulations discussed in this note include pile-up events, as said in Section 3. As a cross-check the analysis was also performed on samples without pile-up simulation, in order to estimate its effect on the selection. As the analyses are based on very high energy SC in the ECAL, very small difference is expected. The main effect indeed comes from vertex reconstruction, which has a higher fake rate when pile-up events are taken into account.

5.3 Significance

The discovery potential of a given new physics resonance is determined using the likelihood estimator S based on event counting [27], suited for small event samples:

$$S = \sqrt{2[(N_{\rm s} + N_{\rm b})\log(1 + \frac{N_{\rm s}}{N_{\rm b}}) - N_{\rm s}]}, \tag{6}$$

where $N_{\rm s}$ (resp. $N_{\rm b}$) is the number of signal (resp. background) events. The discovery limit is defined by $S > 5$.

The numbers of expected signal and background events for an integrated luminosity of 30 fb^{-1} are given in Table 3 for the three considered models, together with the corresponding significances. The significances as a function of the resonance mass are given in Figs. 10(a) and (b) and in Fig. 11 for KK Z boson, Z' boson, and two cases of graviton production, respectively. Those significances are evaluated on the pure statistical basis.

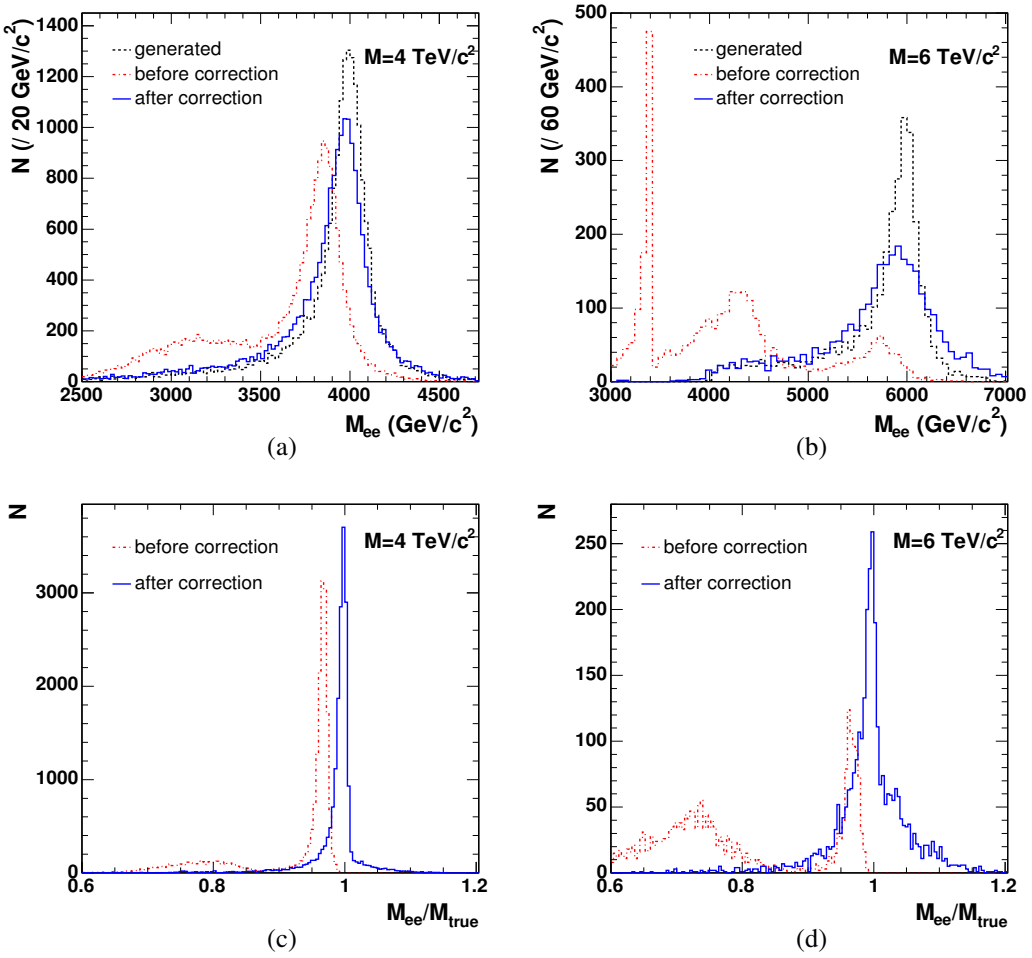

Figure 6: Distributions of the di-electron invariant mass for KK Z boson production with $M = 4$ TeV/c^2 (a) and $M = 6$ TeV/c^2 (b). The dashed lines correspond to the generated distributions, the dashed-dotted lines to the reconstructed distributions before energy and saturation corrections, and the full lines to the corrected distributions. The distributions of the ratio $M_{\rm ee}/M_{\rm true}$ before (dashed line) and after (full line) energy and saturation corrections are given in (c) for $M = 4$ TeV/c^2 and in (d) for $M = 6$ TeV/c^2.

5.4 CMS discovery potential

For KK Z boson production, a 5 σ discovery limit is achieved for compactification scales up to $M = 4.97$ TeV/c^2 for an integrated luminosity of 10 fb^{-1}, $M = 5.53$ TeV/c^2 for 30 fb^{-1} and $M = 5.88$ TeV/c^2 for 60 fb^{-1}. For the graviton production, a 5 σ discovery can be achieved with an integrated luminosity of 30 fb^{-1}, for graviton masses up to 1.64 TeV/c^2 for $c = 0.01$ and up to 3.81 TeV/c^2 for $c = 0.1$. For Z' production, with an integrated luminosity of 30 fb^{-1}, the 5 σ discovery limits are for mass of 3.31 TeV/c^2 for the ψ model and 4.27 TeV/c^2 for the ARLM model. The 5 σ discovery limits on the resonance masses, for the three models and luminosities of 10, 30 and 60 fb^{-1} are summarised in Table 4.

The 5 σ discovery limit is given as a function of the mass in Fig. 12 for KK Z boson production and in Fig. 13 for Z' production. The discovery limits for Z' production are similar to those achieved in the di-muon decay mode [16]. For graviton production, the 5 σ discovery plane is given in Fig. 14, as a function of the graviton mass and the coupling parameter c.

For KK Z boson production, the luminosities needed for a 5 σ discovery, assuming a calibrated and aligned detector, are 1.5, 4.0, 10.8, 29.4, and 81.4 fb^{-1} for M =4.0, 4.5, 5.0, 5.5 and 6.0 TeV/c^2, respectively; for SSM Z' production, they are 0.015, 3.0 and 260 fb^{-1} for $M = 1$, 3 and 5 TeV/c^2; for graviton production, most of the interesting region of the (mass, coupling) plane is already covered with 10 fb^{-1}.

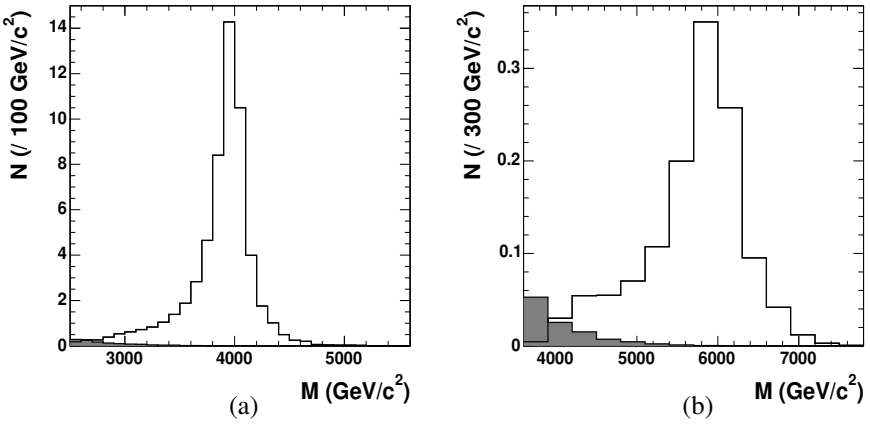

(a) (b)

Figure 7: Resonance signal (white histogram) and Drell-Yan background (shaded histogram) for KK Z production for $M = 4$ TeV/c^2 (a) and $M = 6$ TeV/c^2 (b), for an integrated luminosity of 30 fb^{-1}.

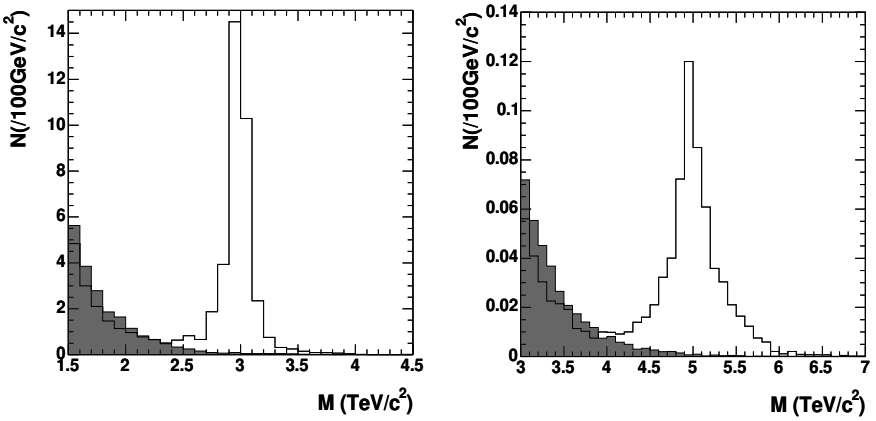

(a) (b)

Figure 8: Resonance signal (white histogram) and Drell-Yan background (shaded histogram) for SSM Z' boson production for $M = 3.0$ TeV/c^2 (a) and $M = 5.0$ TeV/c^2 (b), for an integrated luminosity of 30 fb^{-1}.

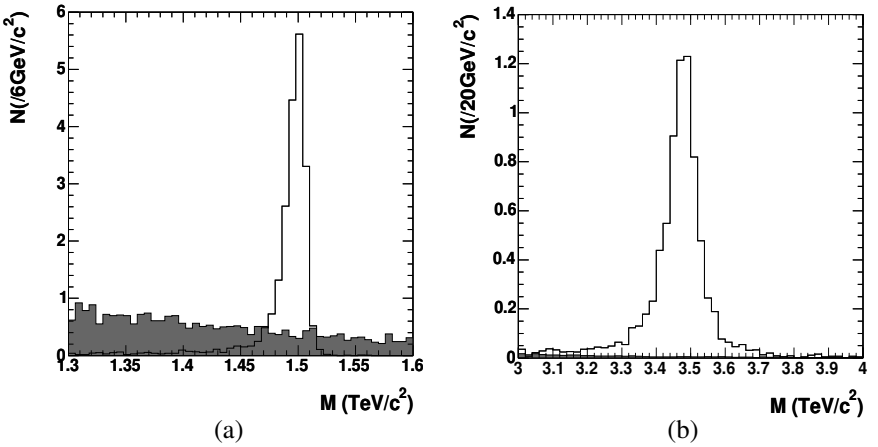

(a) (b)

Figure 9: Resonance signal (white histogram) and Drell-Yan background (shaded histogram) for graviton production with $M = 1.5$ TeV/c^2, $c = 0.01$ (a) and $M = 3.5$ TeV/c^2, $c = 0.1$ (b), for an integrated luminosity of 30 fb^{-1}.

Table 3: Numbers of events for resonant signal, for Drell-Yan background, and corresponding significances as defined by Eq. 6, for an integrated luminosity of 30 fb^{-1}. The masses M and the mass windows M_{w} are in $\mathrm{TeV/c^2}$.

KK Z boson production							
M	4.0	4.5	5.0	5.5	6.0		
M_{w}	3.5-4.5	4.0-5.0	4.4-5.5	4.8-6.0	5.0-6.7		
N_S	50.6	18.4	7.0	2.70	1.05		
N_B	0.13	0.043	0.017	0.007	0.005		
S	22.5	13.7	8.4	5.2	3.0		
G production, weak coupling $c = 0.01$							
M	0.75	1.0	1.25	1.50	1.750	2.0	2.5
M_{w}	0.737-0.762	0.984-1.015	1.228-1.268	1.474-1.521	1.717-1.774	1.962-2.026	2.447-2.533
N_S	612.5	156.1	49.4	18.8	7.98	3.55	0.87
N_B	67.6	21.1	8.8	4.16	2.16	1.17	0.42
S	43.8	21.0	11.0	6.39	3.93	2.47	1.08
G production, strong coupling $c = 0.1$							
M	2.0	2.5	3.0	3.5	4.0	4.5	
M_{w}	1.904-2.080	2.372-2.600	2.846-3.114	3.305-3.641	3.767-4.173	4.099-4.829	
N_S	341	84.7	23.6	7.30	2.41	0.855	
N_B	3.0	1.00	0.307	0.12	0.041	0.032	
S	50.9	24.4	12.7	6.83	3.90	2.06	
SSM Z' boson production							
M	1.0	3.0	5.0				
M_{w}	0.921-1.074	2.726-3.235	4.178-5.820				
N_S	7202	32.5	0.575				
N_B	85.5	0.33	0.025				
S	225	15.4	1.63				

Table 4: Five σ discovery limits on the resonance mass (in $\mathrm{TeV/c^2}$) for three production models, for integrated luminosities of 10, 30 and 60 fb^{-1}.

Model	Luminosity (fb^{-1})		
	10	30	60
KK Z	4.97	5.53	5.88
G ($c = 0.01$)	1.38	1.64	1.82
G ($c = 0.1$)	3.34	3.81	4.10
Z' (ψ)	2.85	3.31	3.62
Z' (ALRM)	3.76	4.27	4.60

6 Identification of the new particles

Once a resonance is found, information will be gained on its characterisation from the study of other decay channels, like $\gamma\gamma$ [18], of angular distributions and of asymmetries in view of the spin determination (see also [19]).

As an example, RS gravitons with spin 2 can be distinguished from the Standard Model background and Z' bosons with spin 1 using the distribution of the $\cos\theta^*$ variable, computed as the cosine of the polar angle between the electron and the boost direction of the heavy particle in the latter rest frame. In addition to the cuts defined above, the electron and positron candidates are requested to have opposite charges, in order to identify the electron, from which the $\cos\theta^*$ variable is computed.

The $\cos\theta^*$ distributions for graviton production with M = 1.0, 1.25 and 1.5 $\mathrm{TeV/c^2}$, $c = 0.01$, and $M = 2.0$, 2.5, and 3.0 $\mathrm{TeV/c^2}$, $c = 0.1$, are presented in Fig. 15, for an integrated luminosity of 100 fb^{-1}. The error bars represent the corresponding statistical uncertainties, applied to the signal distribution obtained from a large statistics simulation. The spin-2 hypothesis (composed by the RS signal in addition to the expected background) is com-

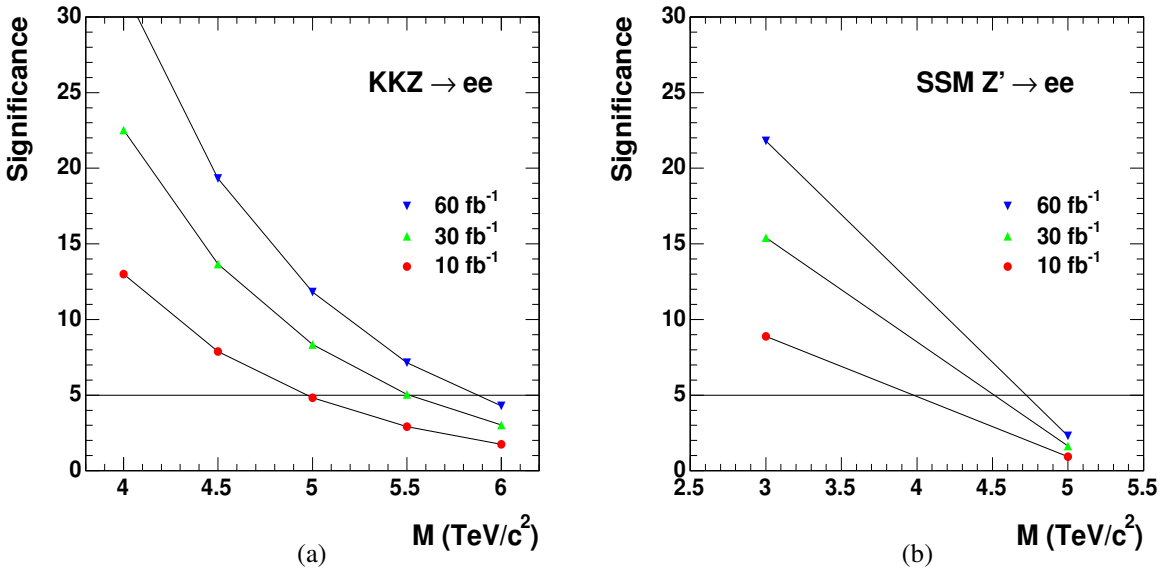

Figure 10: Signal significances as a function of the mass for KK Z boson production (a) and for SSM Z' production (b), for integrated luminosities of 10, 30 and 60 fb^{-1}.

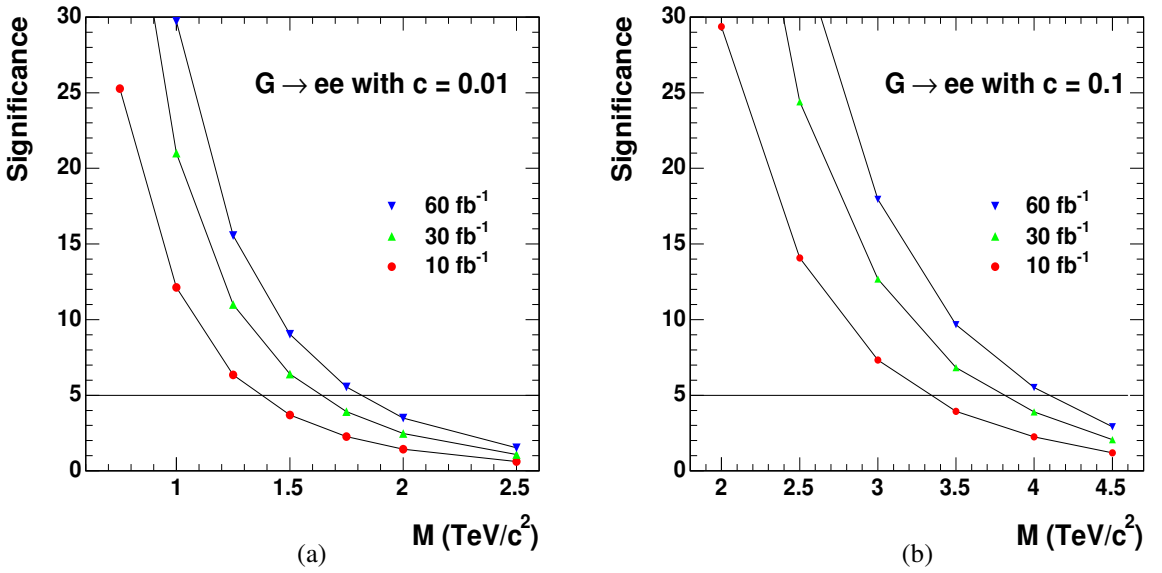

Figure 11: Signal significances as a function of the mass for graviton production for $c = 0.01$ (a) and $c = 0.1$ (b), for integrated luminosities of 10, 30 and 60 fb^{-1}.

pared to the spin-1 hypothesis, formed by the Drell-Yan background (dotted curve in the figure). Figure 16 presents the RS spin-2 hypothesis distribution compared to the spin-1 hypothesis formed by the ALRM Z' production for M = 1.25 $\mathrm{TeV/c^2}$ ($c = 0.01$) and M = 2.5 $\mathrm{TeV/c^2}$ ($c = 0.1$), and for an integrated luminosity of 100 fb^{-1}.

The spin 2 of RS gravitons can be determined by contrast with the Drell-Yan production or the Z' boson production for an integrated luminosity of 100 fb^{-1} up to 1.25 TeV/c^2 for $c = 0.01$ and 2.5 TeV/c^2 for $c = 0.1$.

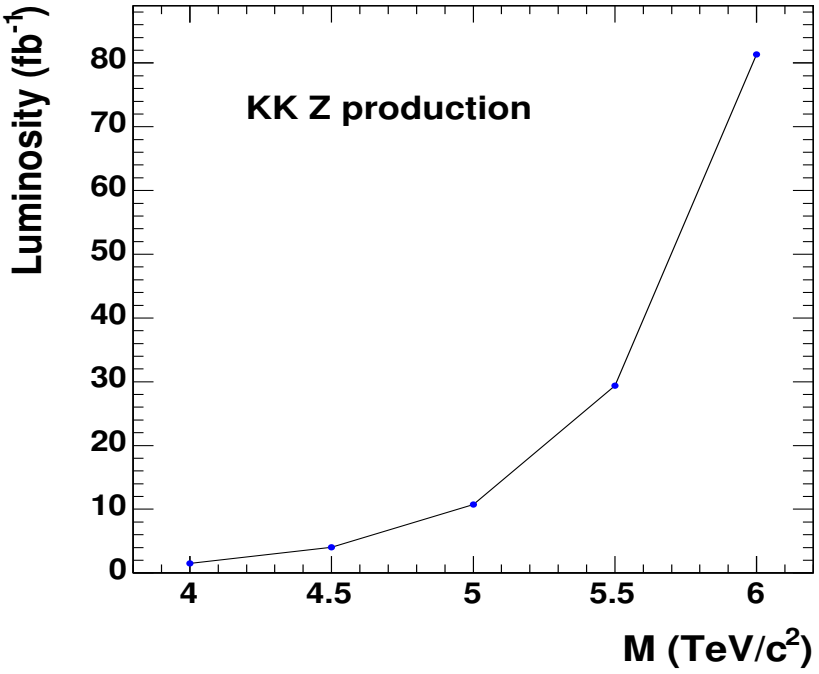

Figure 12: Five σ discovery limit for KK Z boson production.

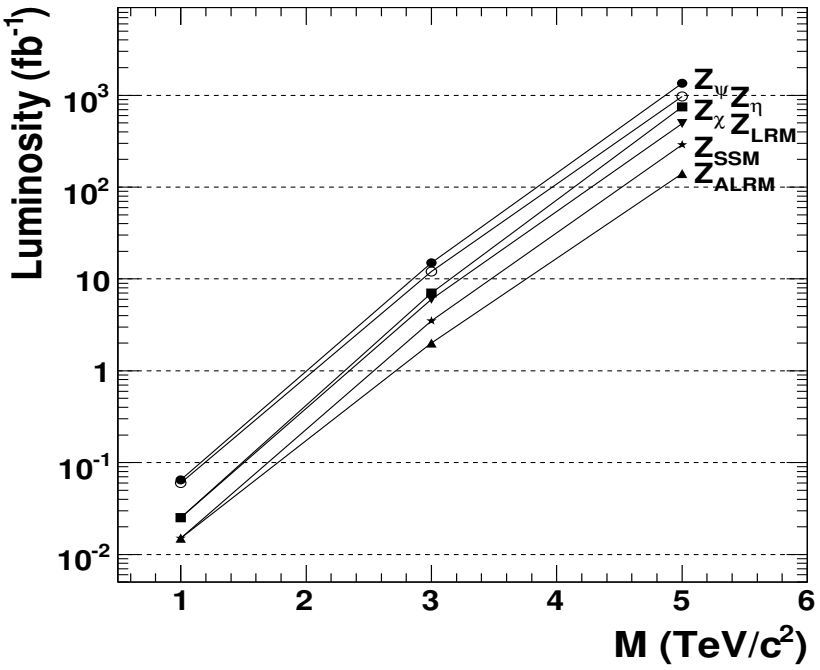

Figure 13: Five σ discovery limit for the 6 Z' production models.

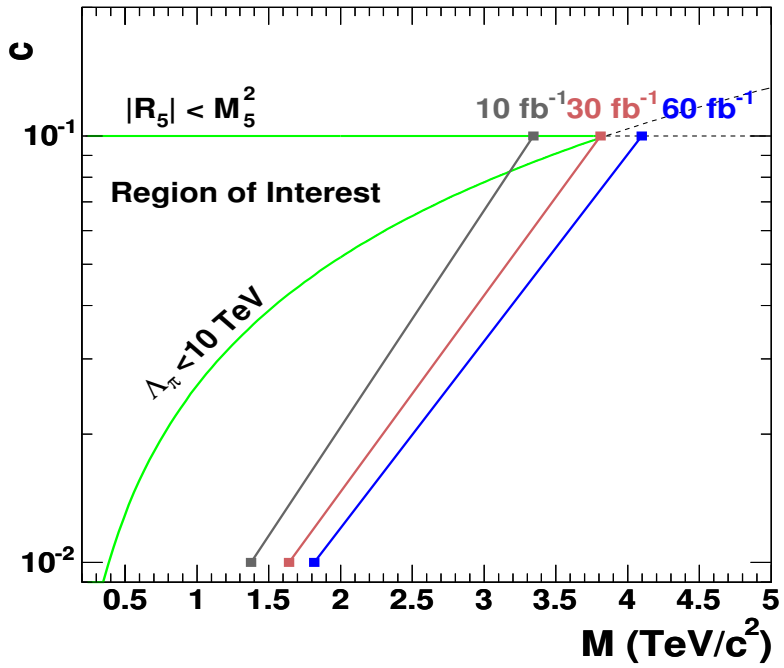

Figure 14: Five σ discovery plane for graviton production, as a function of the graviton mass and the coupling parameter c.

7 Systematic uncertainties

The uncertainty coming from the choice of the parton distribution function (PDF) was investigated using the set of 20 positive and 20 negative errors, of the CETQ6.1M "best fit" parametrisation [21]. For each event, a weight factor is computed according to the x_1, x_2, and Q^2 variables, for each of the 40 PDF errors, in the case of graviton production with $M = 1.5$ TeV/c^2 ($c = 0.01$) and $M = 3.5$ TeV/c^2 ($c = 0.1$). The uncertainties on the PDF modify the number of signal events by a factor 1.20 (positive deviations) and 0.86 (negative deviations) for $M = 1.5$ TeV/c^2 ($c = 0.01$). The corresponding numbers for $M = 3.5$ TeV/c^2 ($c = 0.1$) are 1.47 and 0.78. For the Drell-Yan background, the reweighting effects on the numbers of events are 1.065 and 0.941 for masses around 1.5 TeV/c^2 , and 1.19 and 0.88 for masses around 3.5 TeV/c^2. For an integrated luminosity of 30 fb^{-1}, the significances with the "best fit" and with the positive/negative deviations are equal respectively to 6.40 and 7.25/5.78 for $M = 1.5$ TeV/c^2, and to 6.83 and 8.54/5.93 for $M = 3.5$ TeV/c^2. The main effect of the variation comes from the gluon-fusion contribution to the graviton production cross section. A lower dependence is observed for the KK Z and Z' channels, which are produced by quark-antiquark annihilation. For KK Z boson production at $M = 4$ TeV/c^2 with an integrated luminosity of 30 fb^{-1}, the significances with the "best fit" and with the positive/negative errors are equal respectively to 22.5 and 23.3/21.9.

Changing to 1 the value of the K factor of the DY background for RS graviton production increases the significance from 6.39 to 6.87 ($M = 1.5$ TeV/c^2 , $c = 0.01$) and from 6.83 to 7.09 ($M = 3.5$ TeV/c^2 , $c = 0.1$). The discovery limits increase respectively from 1.64 to 1.68 TeV/c^2 and from 3.81 to 3.84 TeV/c^2.

The data themselves will be used to estimate and cross-check the Drell-Yan background at very high energy. For resonance discovery, the number of events in the side-bands of the resonance and their mass dependence will be used to estimate the number of background events under the resonance peak, provided there is enough data in the side-bands. In this approach, the uncertainties on the background cross-sections, the PDF and the luminosity measurement are highly reduced. Moreover, new phenomena can be involved at dilepton masses which have never been experimentally accessible before the LHC. One example is the ADD extra dimensions mechanism, which in the KK excitations of the graviton appear as a large number of states, degenerated in mass. It gives an excess of dilepton events which increases the cross section of the final state by about a factor 10 compared to DY, in the region of 3 TeV, assuming $M_s = 4$ TeV/c^2 [28].

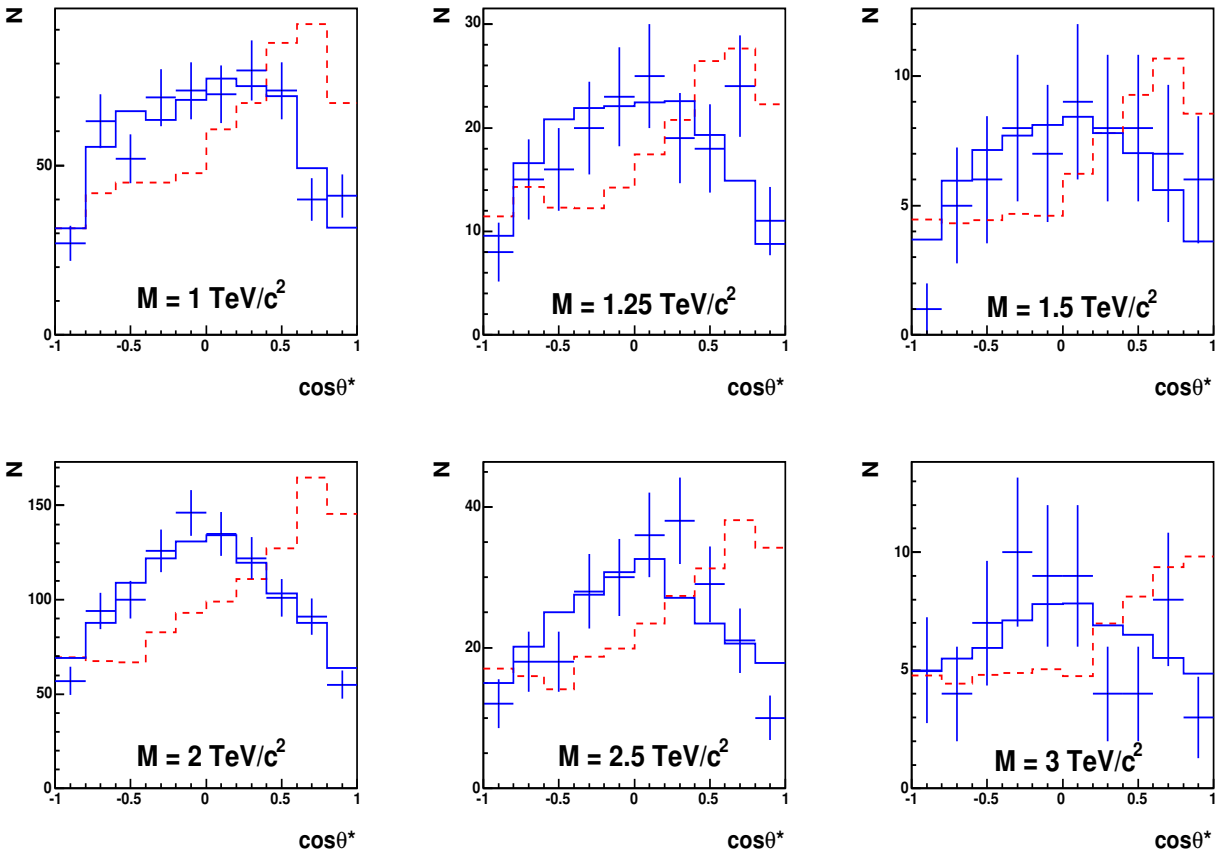

Figure 15: Distributions of $\cos\theta^*$ for graviton production (full curves) and for Drell-Yan production (dotted curves) normalised to the signal, for M = 1.0, 1.25 and 1.5 $\mathrm{TeV/c^2}$ for $c = 0.01$ (top plots), and for $M = 2.0$, 2.5, and 3.0 $\mathrm{TeV/c^2}$ for $c = 0.1$ (bottom plot), with an integrated luminosity of 100 $\mathrm{fb^{-1}}$. The error bars represent the "1-experiment" distribution for the graviton production. The expected background is included in the $\cos\theta^*$ distributions.

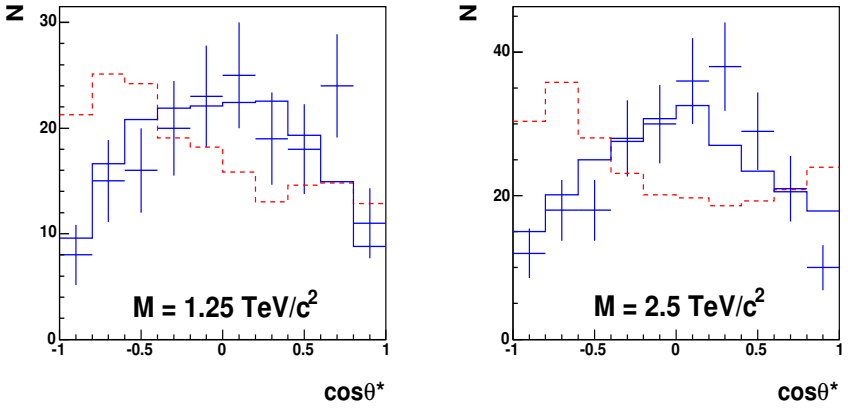

Figure 16: Distributions of $\cos\theta^*$ for graviton production (full curves) and for Z' production (ALRM model) (dotted curves), normalized to the signal, for M = 1.25 $\mathrm{TeV/c^2}$ (a) and 2.5 $\mathrm{TeV/c^2}$ (b), with an integrated luminosity of 100 $\mathrm{fb^{-1}}$. The error bars represent the "1-experiment" distribution for the graviton production. The expected background is included in the $\cos\theta^*$ distributions.

8 Conclusions

This note presents the CMS experiment discovery potential for new heavy resonances decaying into an electron pair. Three models have been considered: Kaluza-Klein excitations of a Z boson (TeV^{-1} model), of a graviton (Randall-Sundrum model) predicted in extra dimensions models and of a neutral heavy Z' boson predicted by Grand Unified Theories.

For an integrated luminosity of 30 fb^{-1}, assuming a calibrated and aligned detector, a 5σ discovery limit has been obtained for masses below 5.5 $\mathrm{TeV/c^2}$ in the case of Kaluza-Klein excitations of a Z boson production. For the Randall-Sundrum graviton production, the limits are found for graviton masses of 1.6 $\mathrm{TeV/c^2}$ with a coupling parameter constant $c = 0.01$ and 3.8 $\mathrm{TeV/c^2}$ for $c = 0.1$. For the six Z' models considered here, the 5 σ discovery limits range for masses from 3.3 $\mathrm{TeV/c^2}$ (Z_ψ) to 4.3 $\mathrm{TeV/c^2}$ ($\mathrm{Z}_{\mathrm{ALRM}}$).

Once a resonance is found, the study of angular distributions provides a way to investigate the nature of the new particle. To distinguish between the different model hypotheses, the $\cos\theta^*$ distribution of Randall-Sundrum graviton production has been compared to the one of Z' production as well as the Drell-Yan production.

Acknowledgments

We would like to thank all the members of the CMS collaboration who contributed to the software programs used for these analyses. We are grateful to F. Beaudette, M.-C. Lemaire and P. Marage for discussions and assistance. We thank the members of the analysis group of the di-muon decay channel at high mass, and in particular V. Valuev, for intensive information exchange. We would also like to thank our referees, F. Beaudette, V. Litvin and L. Malgeri, for their careful reading and valuable comments. T. Mahmoud acknowledges the financial support provided, through the IAP program, by the *Politique scientifique fédérale*, Belgium.

References

[1] N. Arkani-Hamed, S. Dimopoulos and G. Dvali, "The Hierarchy Problem and New Dimensions at a Millimeter", Phys. Lett. B429 (1998) 263, hep-ph/9803315

[2] J. Hewett and M. Spiropulu, "Particle physics probes of extra spacetime dimensions", Ann. Rev. Nucl. Part. Sci. 52 (2002) 397, hep-ph/0205106

[3] See the review by S. Mele and the presentation by L. Vacavant, http://eps2003.physik.rwth-aachen.de/transparencies/09/index.php

[4] K. Antoniadis, K. Benaki and M. Quiros, "Production of Kaluza-Klein states at future colliders", Phys. Lett. B331 (1994) 312

[5] T.G. Rizzo, "Testing the nature of Kaluza-Klein excitations at future lepton colliders", Phys. Rev. D61 (2000) 055005, hep-ph/9909232

[6] G. Azuelos and G. Polesello, "Beyond the standard model working group: Summary report", hep-ph/0204031

[7] K.R. Dienes, E. Dudas and T. Gherghetta, "Grand unification at intermediate mass scales through extra dimensions", Nucl. Phys. B537 (1999) 47, hep-ph/9806292

[8] N. Arkani-Hamed and M. Schmaltz, "Hierarchies without symetries from extra dimensions", Phys.Rev. D61 (2000) 033005, hep-ph/9903417

[9] K. Cheung and L. Landsberg, "Kaluza-Klein States of the Standard Model Gauge Bosons: Constraints From High Energy Experiments", Phys. Rev. D65 (2002) 076003, hep-ph/0110346

[10] L. Randall and R. Sundrum, "A Large Mass Hierarchy from a Small Extra Dimension", Phys. Rev. Lett. 83 (1999) 3370, hep-ph/9905221

[11] W.D. Goldberger and M.B. Wise, "Phenomenology of a stabilized modulus", Phys. Lett. B475 (2000) 275, hep-ph/9911457

[12] P. Verdier, Physics in Collision, Zuethen, Germany, June 2003, hep-ph/0310021;
CDF Collaboration, "Measurement of ds/dM and Forward-Backward Charge Asymmetry for High-mass Drell-Yan $\mathrm{e^+e^-}$ Pairs from collisions at $\sqrt{s} = 1.8$ TeV", Phys. Rev. Lett. 87 (2001) 131802

[13] J. L. Rosner, "Off peak lepton asymmetries from new Zs", Phys. Rev. D35 (1987) 2244

[14] M. Cvetič and S. Godfrey, in: T. L. Barklow (ed.) *et al.*, *Electroweak Symmetry Breaking and New Physics at the TeV Scale* (World Scientific, 1995), 383, hep-ph/9504216;
S. Godfrey, "Update of Discovery Limits for Extra Neutral Gauge Bosons at Hadron Colliders" in *proceedings of the APS/DPF/DPB Summer Study on the Future of particle Physics* (Snowmass, 2001), hep-ph/0201093

[15] For a review, see K. S. Babu and C. Kolda, "The Z' Searches" in the Review of Particles Physics, Phys. Lett. B592 (2004) 380

[16] R. Cousins, J. Mumford and V. Valuev, "Detection of Z' Gauge Bosons in the Dimuon Decay Mode in CMS", CMS NOTE 2005-002

[17] C. Collard and M.-C. Lemaire, "Search with the CMS Detector for Randall-Sundrum Excitations of Gravitons Decaying Into Electron Pairs", CMS NOTE 2004-024

[18] M.-C. Lemaire, V. Litvin and H. Newman, "Search for Randall-Sundrum excitations of gravitons decaying into two photons for CMS at LHC", CMS NOTE 2006-051

[19] R. Cousins, J. Mumford and V. Valuev, "Forward-Backward Asymmetry of Simulated and Reconstructed Z'$\rightarrow \mu^+\mu^-$ Events in CMS", CMS NOTE 2005-022

[20] T. Sjöstrand *et al.*, Computer Phys. Commun. 135, 238 (2001), LU TP 00-30, hep-ph/0010017

[21] CTEQ Collaboration, H.L. Lai *et al.*, Eur. Phys. J. C12 (2000) 375;
J. Pumplin *et al.*, JHEP 0207 (2002) 012, hep-ph/0201195;
D. Stump *et al.*, JHEP 0310 (2003) 046, hep-ph/0303013

[22] E. Barberio and Z. Was, Computer Physics Commun. 79, 291 (1994)

[23] R. Hamberg, W.L. van Neerven and T. Matsuura, "A Complete calculation of the order alpha-s**2 correction to the Drell-Yan K factor", Nucl. phys. B359 (1991) 343,
erratum: R. Hamberg, W.L. van Neerven and T. Matsuura, Nucl. phys. B644 (2002) 403

[24] E. Meschi *et al.*, CMS NOTE 2001-034

[25] M. Raymond, J. Crooks, M. French and G. Hall, "The MGPA Electronic Calorimeter Readout Chip for CMS", Proceeding of the 2003 LECC Conference, CERN-2003-006

[26] B. Clerbaux *et al.*, "TeV electron and photon saturation studies", CMS NOTE 2006-004

[27] V. Bartsch and G. Quast, "Expected signal observability at future experiments", CMS NOTE 2005-004

[28] V. Kabachenko *et al.*, ATL-PHYS-2001-012;
O.J.P. Eboli *et al.*, Phys. Rev. D61 094007 (2000)